JOURNAL OF SOLID STATE CHEMISTRY 37, 189–203 (1981)

Neutron Powder Diffraction and Magnetic Measurements on $TlMnI_3$ and $TlFeI_3$

H. W. ZANDBERGEN

Gorlaeus Laboratories, University of Leiden, P.O. Box 9502, 2300 RA Leiden, The Netherlands

Received March 26, 1980; in revised form June 26, 1980

$TlMnI_3$ and $TlFeI_3$ are isostructural with NH_4CdCl_3. $TlMnI_3$ has a spiral structure which can be described with an incommensurable vector **k**, in the direction of the **b*** axis of length 0.3614(5)**b***. The spins lie in the (0 0 1) plane. $TlMnI_3$ exhibits antiferromagnetic behavior with a Néel temperature of 6.0(2) K. The exchange interaction was calculated to be $zJ/k = -1.6$ K, z being the number of nearest neighbors. Discontinuities in the magnetization are found for both the [1 0 0] and [0 1 0] directions at fields $H_{\S_F} = 30.1(2)$ kOe and $H_{\S_F} = 14.1(2)$ kOe. The magnetic structure of $TlFeI_3$ consists of puckered ferromagnetic (1 0 0) planes, which are coupled antiferromagnetically. The magnetic moments are parallel to the b axis. The Néel temperature is 21.5(3) K. zJ/k was found to be $-10(1)$ K with $g = 2.68$ and $s = 2$. The magnetic structures found for $TlMnI_3$ and $TlFeI_3$ are derived taking into account inter- and intra-double-chain interactions via two I^- ions.

Introduction

The phase diagram of TlI–MnI_2 is reported by Seifert and Kischka (*1*). Two compounds exist in this phase system: $TlMnI_3$, which melts incongruently at 368°C (*1*) and adopts the NH_4CdCl_3 structure (*1*, *2*), and Tl_4MnI_6, which melts congruently at 362°C (*1*) and is isostructural to Tl_4CrI_6 (*3*). In the phase system TlI–FeI_2 compounds with the same composition do occur: $TlFeI_3$, which melts incongruently at 262°C, adopting the NH_4CdCl_3 structure, and Tl_4FeI_6, which is isostructural to Tl_4CrI_6 and melts congruently at 318°C. Some other iodides, $TlCdI_3$ (*2*), $KPbI_3$ (*2*), $RbPbI_3$ (*4*), and $CsPbI_3$ (*5*) also adopt the NH_4CdCl_3 structure.

It is interesting to investigate the magnetic structure and the magnetic interactions in $TlMnI_3$ and $TlFeI_3$. The compounds consist of double chains so that the exchange interactions can be divided into intra- and inter-double-chain interactions. The ratio of these interactions will determine the dimensionality of the compounds.

Experimental

The sample of $TlMnI_3$ used for neutron diffraction was prepared by melting a stoichiometric mixture of the binary compounds and—after powdering—annealing at 350°C for 3 weeks. The sample of $TlFeI_3$ was prepared in a similar way but in this case the sample had to be powdered and annealed at 250°C several times to obtain a pure sample. Although $TlMnI_3$ melts incongruently, it was possible to grow transparent single crystals from a stoichiometric

0022-4596/81/050189-15$02.00/0

mixture of the binary compounds using the Bridgman method. For $TlFeI_3$ only a collection of single crystals of $TlFeI_3$, all with their b axis in about the same direction, was obtained using the Bridgman method. For both compounds the b axis is the direction most favored for crystal growth. Since both title compounds are very hygroscopic, all manipulations were carried out in a dry glovebox in argon. The starting materials for all preparations were purified by distillation (TlI) or sublimation (MnI_2 and FeI_2).

Powder neutron diffraction diagrams were recorded at the HFR at Petten (the Netherlands), using the wavelength λ = 2.5718(3) Å with 30′ collimation, at 293 K for both compounds and 1.2 and 4.2 K for $TlMnI_3$ and $TlFeI_3$ respectively in the angular range $4° < 2\Theta < 140°$. No absorption correction was applied. The coherent scattering lengths (*6*) used are: $b(Tl) = 0.89$, $b(Mn) = -0.37$, $b(Fe) = 0.95$, and $b(I) = 0.53$, all in units of 10^{-12} cm. The magnetic form factors were taken from Watson and Freeman (*7*). The refinements of the structures from the neutron diffraction data have been performed by means of the profile refinement method (*8*).

Magnetic measurements were carried out by means of a vibrating-sample magnetometer equipped with a superconducting magnet, supplying fields up to 56 kOe (*9*).

Refinements of the Neutron Diffraction Data

$TlMnI_3$ (293 K)

In the refinement of the neutron diffraction data recorded at 293 K, the positional parameters of $TlCdI_3$ (*2*) were taken as starting values. Full matrix refinement of the unit cell parameters and the positional and isotropic thermal parameters for all ions in space group *Pnma* led to convergence at

$$R(\text{total}) = \sum_i |I_i(\text{obs}) - (1/c)I_i(\text{calc})| \Big/ \sum_i I_i(\text{obs}) = 0.044$$

and

$$R(\text{profile}) = \left\{ \sum_j w_j (y_j(\text{obs}) - (1/c)y_j(\text{calc}))^2 \Big/ \sum_j w_j (y_j(\text{obs}))^2 \right\}^{1/2} = 0.095,$$

where I_i is the intensity of the ith reflection, y_j the intensity of the jth measuring point, w_j a statistical weight factor, and c a scaling factor; the ratio of parameters to reflections, $n(\text{par})/n(\text{refl})$, is 24/274. Refinement in space group $Pn2_1a$ did not lead to significantly lower R values or significantly different positions. Figure 1

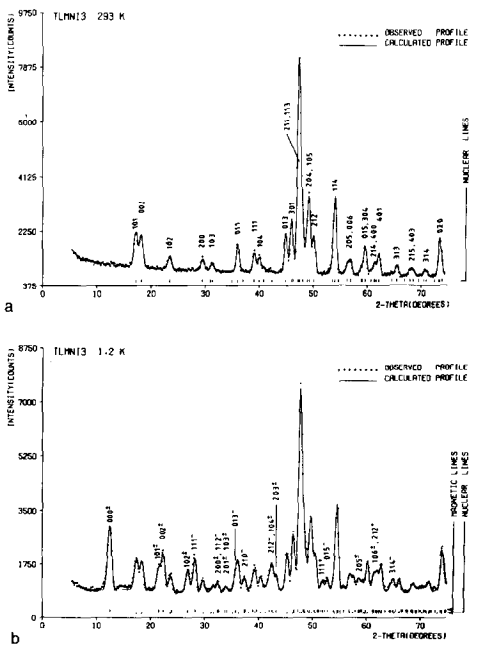

FIG. 1. The observed and calculated diffraction profiles of $TlMnI_3$ at 293 K (a) and 1.2 K (b) up to 70°.

shows the observed and calculated diffraction profiles. The positional and thermal parameters and the unit cell dimensions are listed in Table I. Some distances and bond angles are given in Table II.

$TlMnI_3$ (1.2 K)

The neutron diffraction pattern recorded at 1.2 K contains a large number of magnetic reflections. These cannot be indexed satisfactorily on the basis of simple multiples of the nuclear cell. Because several competing exchange interactions exist, a spiral structure might occur.

In a spiral structure there is no simple relation between the translation period of the magnetic structure and that of the nuclear structure. A spiral structure can be described in reciprocal space by a vector **k**.

All reflections of magnetic origin could be indexed on the basis of

$$(4/\lambda^2)\sin^2\theta = h^2|\mathbf{a}^*|^2 + (k|\mathbf{b}^*| \pm |\mathbf{k}|)^2 + l^2\mathbf{c}^{*2},$$

where h, k, l are Miller indices; $\mathbf{a}^*$, $\mathbf{b}^*$, $\mathbf{c}^*$ are the reciprocal axes; and **k** is an incommensurable vector in the $\mathbf{b}^*$ direction. The

TABLE I

POSITIONAL AND ISOTROPIC THERMAL PARAMETERS, MAGNETIC MOMENT, AND UNIT CELL DIMENSIONS OF $TlMnI_3$ AT 293 AND 4.2 K

	x	y	z	b^a (Å²)	μ (μ_B)
293 K (a = 10.074(1), b = 4.2967(5), c = 16.172(2) Å)					
Tl	0.4418(5)	0.25	0.1753(3)	3.7(1)	
Mn	0.1628(9)	0.25	0.9421(6)	2.3(2)	
I(1)	0.2810(6)	0.25	0.7884(4)	1.0(2)	
I(2)	0.1692(5)	0.25	0.5079(4)	1.1(2)	
I(3)	0.0245(6)	0.25	0.1052(4)	0.8(2)	
4.2 K (a = 9.991(2), b = 4.2701(8), c = 16.020(3) Å)					
Tl	0.4454(7)	0.25	0.1745(4)	0.8(2)	
Mn	0.1626(9)	0.25	0.9439(6)	0.8(2)	4.61(4)
I(1)	0.2834(9)	0.25	0.7857(6)	0.0(3)	
I(2)	0.1670(10)	0.25	0.5078(5)	−0.1(3)	
I(3)	0.0216(9)	0.25	0.1049(5)	−0.2(2)	

[a] $b = 8\pi^2\bar{U}^2$ Å² (*19*).

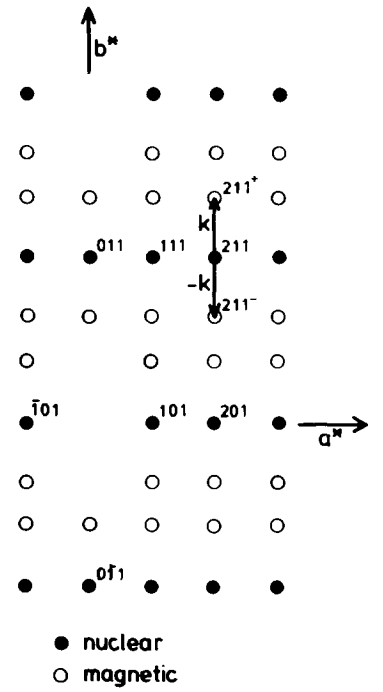

FIG. 2. The (h k 1) plane of the reciprocal lattice of $TlMnI_3$. The nuclear lattice points have magnetic satellites at the positions +**k** and −**k**. The systematically absent reflections are omitted.

length of **k** is 0.3614(5)$\mathbf{b}^*$. This implies, for every nuclear, reciprocal lattice point, two satellites at distances +**k** and −**k**, denoted as hkl^+ and hkl^- (see Fig. 2). Only satellites of allowed nuclear reflections were found, indicating that the phases of the four spirals in the unit cell are equal.

Unfortunately the profile program used does not allow the introduction of an incommensurable vector **k**. Therefore **k** = (4/11)$\mathbf{b}^*$ (which is equal to 0.3636$\mathbf{b}^*$) was taken instead of **k** = 0.3614$\mathbf{b}^*$. This **k** can be introduced in the refinement program by multiplying the b axis by 11 and allowing only the reflections hkl with $k = 11n \pm 4$ (magnetic) or $k = 11n$ (nuclear).

Three spin planes, (0 0 1), (0 1 0), and (1 0 0), with an equal phase in both double chains were introduced in the refinement. The best fit to the diffraction data was obtained with the model in

TABLE II

SOME RELEVANT DISTANCES (Å) AND BOND ANGLES (DEGREES) OF $TlMnI_3$

	293 K	1.2 K
Distance		
Mn–I(1)	2.76(1)	2.81(1)
Mn–I(2)	2.93(1)	2.92(1)
Mn–I(3)	2.96(1)	2.93(1)
Mn–I(3)	2.98(1)	2.94(1)
Tl–I(1)	3.61(1)	3.60(1)
Tl–I(1)	3.57(1)	3.51(1)
Tl–I(2)	3.63(1)	3.60(1)
Tl–I(2)	3.75(1)	3.66(1)
Tl–I(3)	3.65(1)	3.61(1)
Tl–I(3)	4.35(1)	4.38(1)
I(1)–I(3)	4.15(1)	4.09(1)
I(3)–I(3)	4.04(1)	3.97(1)
Mn–Mn	4.34(2)	4.28(2)
Bond angle		
Mn–I(2)–Mn	94.1(3)	94.1(4)
Mn–I(3)–Mn	94.0(3)	93.8(3)
Mn–I(3)–Mn	93.1(3)	93.8(4)
Mn–I(1)–I(3)	148.0(1)	148.0(1)
Mn–I(2)–I(2)	137.4(1)	137.1(2)
Mn–I(2)–I(2)	148.6(3)	148.6(3)
Mn–I(3)–I(1)	149.4(3)	149.4(3)
Mn–I(3)–I(3)	136.6(2)	136.5(2)

which the magnetic moments are in the (0 0 1) plane. Because of indications from the magnetic measurements, the refinement was repeated with the angle between the spin plane and (0 0 1) as a parameter. The value obtained was 1(2)°. Hence it is concluded that the spins are in the (0 0 1) plane within the limits of error.

A correction has been applied for the anisotropy since the anisotropy fields are known from the magnetization vs the magnetic field measurements. The direction of the nth Mn^{2+} ion is determined by $\mathbf{H}_A + \mathbf{H}_E$, $\mathbf{H}_A$ being the anisotropy field and $\mathbf{H}_E$ the antiferromagnetic exchange field (see Fig. 3). $\mathbf{H}_E$ is assumed to be of the same magnitude on all Mn^{2+} sites and that the direction of $\mathbf{H}_E$ changes in proportion to the rotation angle of the spiral. Denoting the angle between $\mathbf{H}_E$ and the a axis by γ and the angle between $\mathbf{H}_A + \mathbf{H}_E$ and the a axis by γ', γ' can be calculated with

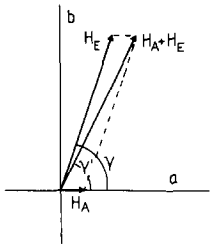

FIG. 3. Definition of the angles γ and γ' used for the correction on the spin direction for alignment along the a axis due to anisotropy.

$$1/\tan \gamma' = 1/\tan \gamma + \mathbf{H}_A/\mathbf{H}_E.$$

Introduction of γ' instead of γ results in a drop of the magnetic R factor from 8.28 to 7.23%. The final R values for refinement with the magnetic moments in the (0 0 1) plane and a correction for the anisotropy are R(total) = 0.059, R(nuclear) = 0.057, R(magnetic) = 0.072, and R(profile) = 0.115 with n(par)/n(refl)

TABLE III

POSITIONAL AND ISOTROPIC THERMAL PARAMETERS, MAGNETIC MOMENT, AND UNIT CELL PARAMETERS OF $TlFeI_3$ AT 293 AND 4.2 K

	x	y	z	b^a (Å²)	μ (μ_B)
293 K (a = 9.967(1), b = 4.2407(5), c = 15.981(1) Å)					
Tl	0.4442(5)	0.25	0.1734(3)	3.6(1)	
Fe	0.1619(4)	0.25	0.9458(3)	2.3(1)	
I(1)	0.2772(6)	0.25	0.7885(5)	2.4(2)	
I(2)	0.1714(6)	0.25	0.5068(4)	1.9(2)	
I(3)	0.0222(6)	0.25	0.1043(4)	1.7(2)	
4.2 K (a = 9.884(1), b = 4.2134(5), c = 15.823(1) Å)					
Tl	0.4458(5)	0.25	0.1732(3)	1.5(1)	
Fe	0.1628(3)	0.25	0.9472(3)	1.0(1)	3.80(6)
I(1)	0.2763(6)	0.25	0.7871(6)	0.9(2)	
I(2)	0.1721(6)	0.25	0.5059(4)	0.5(2)	
I(3)	0.0200(6)	0.25	0.1034(4)	0.2(2)	

[a] $b = 8\pi^2\bar{U}^2$ Å² (19).

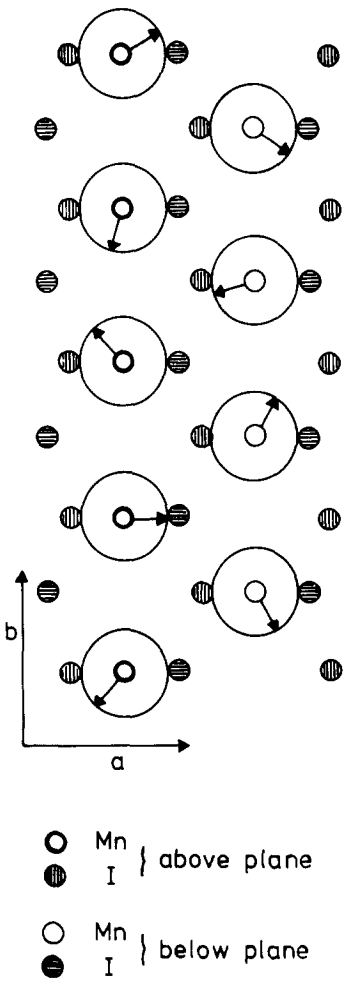

FIG. 4. The spin arrangement in a double chain of $TlMnI_3$ as found by neutron diffraction.

= 25/475. This model is shown in Fig. 4. The results are given in Tables I and II and in Fig. 1.

$TlFeI_3$ (293 K)

Refinement in space group *Pnma* with conditions similar to those of the 293-K refinement of $TlMnI_3$ lead to convergence at R(profile) = 0.098 and R(total) = 0.053; n(par)/n(refl) = 24/271. For this compound as well, refinement in space group $Pn2_1a$ did not lead to significantly lower R values or significant shifts from the positions of the ions in the refinement in space group *Pnma*. The results are given in Tables III and IV and in Fig. 5.

$TlFeI_3$ (4.2 K)

The magnetic reflections in the diagram of the 4.2-K recording of $TlFeI_3$ can all be indexed with a unit cell equal to the nuclear one. Strong (1 0 0) and (0 0 2) reflections occur in the diffraction diagram suggesting the space group to be *Pn'ma* with the magnetic moments parallel to the *b* axis. Refinement with this model led to convergence at R(profile) = 0.086 and R(total) = 0.046 with R(nuclear) = 0.045 and R(magnetic) = 0.051; n(par)/n(refl) = 25/274. The magnetic structure is depicted in Fig. 6. The results are given in Tables III and IV and in Fig. 5.

TABLE IV
SOME RELEVANT DISTANCES (Å) AND BOND ANGLES (DEGREES) IN $TlFeI_3$

	293 K	4.2 K
Distance		
Fe–I(1)	2.76(1)	2.77(1)
Fe–I(2)	2.86(1)	2.82(1)
Fe–I(3)	2.92(1)	2.89(1)
Fe–I(3)	2.89(1)	2.85(1)
Tl–I(1)	3.55(1)	3.52(1)
Tl–I(1)	3.57(1)	3.54(1)
Tl–I(2)	3.59(1)	3.58(1)
Tl–I(2)	3.66(1)	3.61(1)
Tl–I(3)	3.64(1)	3.61(1)
Tl–I(3)	4.35(1)	4.35(1)
I(1)–I(3)	4.14(1)	4.12(1)
I(2)–I(2)	4.03(1)	4.01(1)
Fe–Fe	4.23(1)	4.19(1)
Bond angle		
Fe–I(2)–Fe	95.5(2)	96.6(2)
Fe–I(3)–Fe	93.3(2)	93.7(2)
Fe–I(3)–Fe	93.6(2)	94.0(2)
Fe–I(1)–I(3)	147.9(1)	147.5(1)
Fe–I(2)–I(2)	137.7(1)	138.3(1)
Fe–I(2)–I(2)	149.7(3)	150.3(3)
Fe–I(3)–I(1)	150.6(2)	151.0(2)
Fe–I(3)–I(3)	136.6(1)	136.8(1)

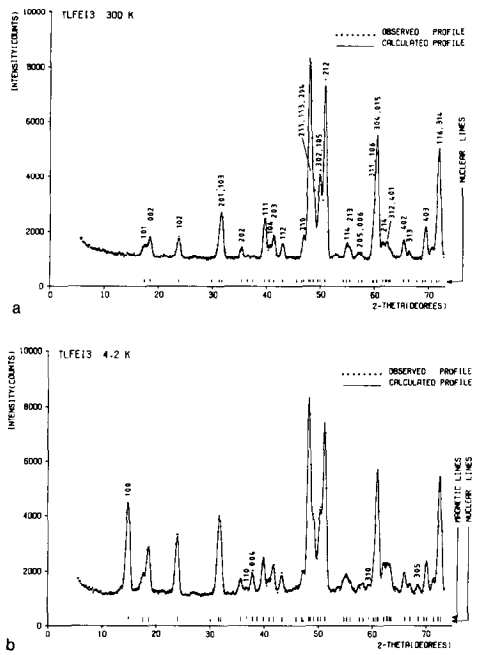

FIG. 5. The observed and calculated diffraction profiles of $TlFeI_3$ at 293 K (a) and 4.2 K (b) up to 70°.

Magnetic Measurements

Samples of $TlMnI_3$ and $TlFeI_3$ Used for the Magnetic Measurements

On a transparent crystal of $TlMnI_3$ weighing 360 mg, χ vs T and M vs H measurements were done. Of this crystal only the direction of the b axis could be determined before the magnetic measurements were performed. By means of a rotation diagram in the a–c plane the orientations of the crystal with maximum and minimum susceptibility were determined. After the magnetic measurements, analysis on an X-ray three-circle diffractometer showed that the crystal contained at least three single crystals in different orientations with a common orientation of the b axis. The average a axis corresponds with the direction in the (0 1 0) plane with minimal χ. In the following this direction will be called the a direction.

On a sample (445 mg) of $TlFeI_3$ composed of needle-shaped crystals mostly oriented in the same direction (the b axis), magnetic measurements were done along three orthogonal directions, viz., the common b axis and the directions in the common (0 1 0) plane with minimal and maximal χ. Analysis by means of X-ray diffraction showed no common a axis—not even in small particles—to exist and impurity of Tl_4FeI_6 to be present.

Magnetization Measurements on $TlMnI_3$

The field dependence of the magnetization was measured up to 56 kOe along the three orthorhombic axes. The magnetization vs magnetic field curves are depicted in Fig. 7. The antiferromagnetic exchange field, H_E, is estimated to be about 53 kOe from the slope of the magnetization vs magnetic field curves (using the molecular field relation $\chi_\perp = N_0 g \mu_B S/2H_E$). For comparison the exchange field calculated from the antiferromagnetic interaction $zJ/k = -1.6$ K (as determined from fits on the χ vs T curves) $H_E = 2z|J|S/g\mu_B$, and using $g = 2$, amounts to $H_E = 55$ kOe.

Spin reorientations occur with fields along the a and b axes. Our interpretation is that with a field parallel to the a axis the spins flop from an orientation in the (0 0 1) plane to an orientation in the (1 0 0) plane and similarly for a field parallel to the b

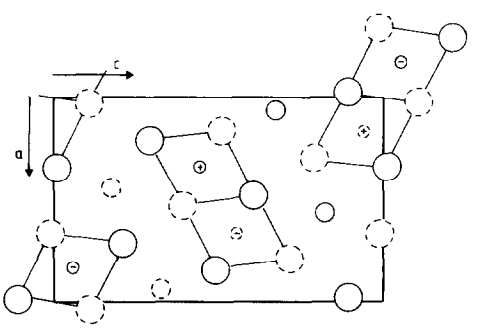

FIG. 6. A (0 1 0) projection of the magnetic structure of $TlFeI_3$. The magnetic moments are parallel to the b axis and point from or to the (0 1 0) plane (indicated by + or −).

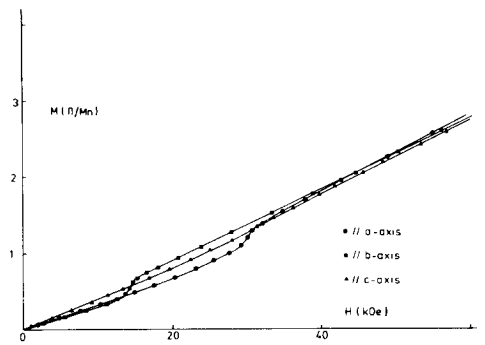

FIG. 7. The magnetization vs the magnetic field curves along the three orthorhombic axes of $TlMnI_3$ at 2.0 K.

axis. At fields above the spin flop, a spiral structure will probably still exist since the exchange interaction leading to a spiral structure is larger than the anisotropy. In the [1 0 0] direction the spin-flop field, H^a_{SF}, is 30.1(2) kOe and in the [0 1 0] direction, $H^b_{SF} = 14.1(2)$ kOe.

For this spin-flop model the anisotropy fields can be calculated. Since $TlMnI_3$ has a spiral structure, the magnetic lattice can be divided into a large number of sublattices; the actual number depends on the matching of the magnetic periodicity with the nuclear one. Each sublattice has a magnetization $\mathbf{M}_i$. Assuming that the sublattice susceptibilities perpendicular to $\mathbf{M}_i$ ($\chi^s_\perp$) are all equal, as well that the sublattice susceptibilities parallel to $\mathbf{M}_i$ ($\chi^s_\parallel$) are equal, the free energy of the system can be written as

$$F = (1/2N)\sum_{i=1}^{N}[-(\chi^s_\parallel\cos^2\psi_i - \chi^s_\perp\sin^2\psi_i)H^2 + 2K_1\sin^2(\psi_i - \beta_1) + 2K_2\sin^2(\psi_i - \beta_2)], \quad (1)$$

where K_1 and K_2 are the anisotropy constants along the a and b axes respectively, ψ_i is the angle between the magnetic field $\mathbf{H}$ and the sublattice magnetization $\mathbf{M}_i$, and β_1 and β_2 are the angles between $\mathbf{H}$ and the a axis and b axis, respectively. If $\mathbf{H}$ is parallel to the a axis, $\beta_1 = 0$ and $\beta_2 = \pi/2$, giving

$$F = (1/2N)\sum_{i=1}^{N}[-(\chi^s_\parallel\cos^2\psi_i - \chi^s_\perp\sin^2\psi_i)H^2 + 2K_1\sin^2(\psi_i) + 2K_2\sin^2(\varphi_i)], \quad (2)$$

where φ_i is the angle between $\mathbf{M}_i$ and the b axis. This equation is valid for $H < H^a_{SF}$. If $H > H^a_{SF}$, the free energy will be

$$F = (1/2N)\sum_{i=1}^{N}[-\chi^s_\perp H^2 + 2K_1 + 2K_2\sin^2\varphi_i]. \quad (3)$$

Since at fields above and below the spin-flop field a spiral with its spin plane parallel to the b axis is assumed to be present, the terms $\sum_{i=1}^{N}2K_2\sin^2\varphi_i$ in Eqs. (2) and (3) will be equal when alignments due to anisotropy are neglected. This gives for $H = H^a_{SF}$

$$-\chi^s_\perp H^{a2}_{SF} + 2K_1 = (1/N)\sum_{i=1}^{N}[-(\chi^s_\parallel\cos^2\psi_i + \chi^s_\perp\sin^2\psi_i)H^{a2}_{SF} + 2K_1\sin^2\psi_i]. \quad (4)$$

When we also assume an equal probability for all directions for the sublattice magnetizations, Eq. (4) can be simplified to

$$(\chi^s_\parallel - \chi^s_\perp)H^{a2}_{SF} = 2K_1. \quad (5)$$

This equation is equivalent to the one obtained by Kanamori (*10*) for a collinear system. Following Kanamori, Eq. (5) can be rewritten as

$$H^{a2}_{SF} = 2H^a_A H_E, \quad (6)$$

where H_E is the exchange field and H^a_A is the anisotropy field in the a direction.

For a magnetic field applied along the b axis, a similar equation is obtained.

With Eq. (6) the anisotropy fields along the a and the b axis can be calculated yielding $H^a_A = 8.2(1)$ kOe and $H^b_A = 1.8(1)$

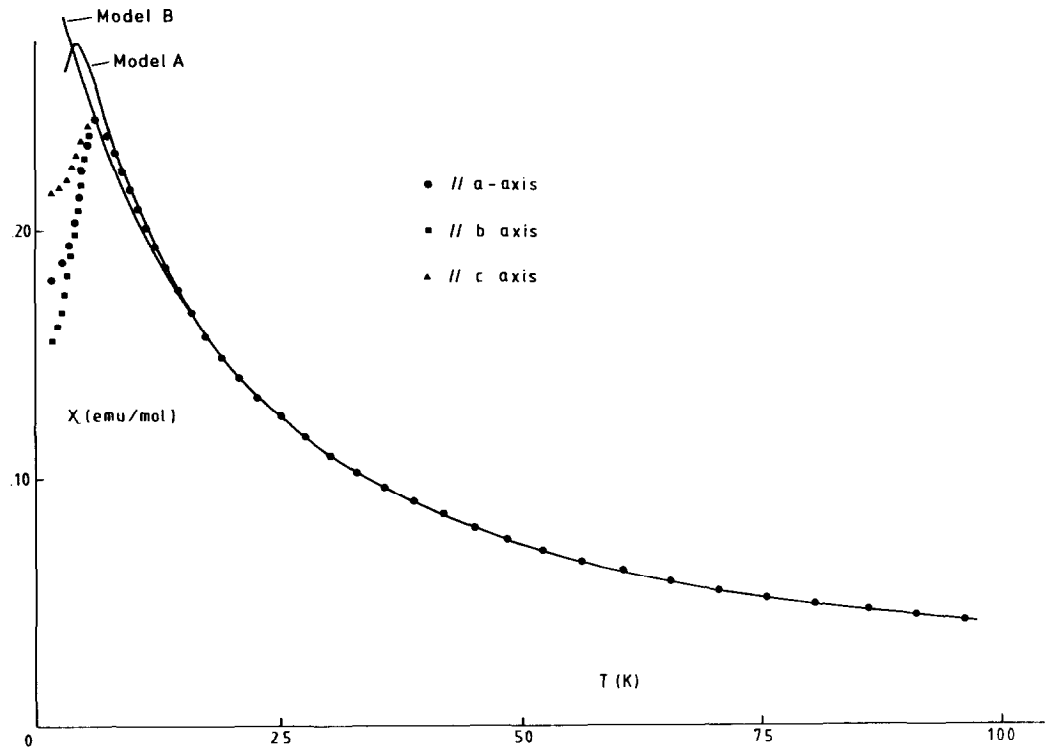

FIG. 8. Susceptibility vs temperature plots along the orthorhombic axes of $TlMnI_3$ at a magnetic field of 1.68 kOe.

kOe. The ratio H_A/H_E, a measure for the deviation from the Heisenberg model, for $TlMnI_3$ is $H_A^a/H_E = 0.149(2)$ and $H_A^b/H_E = 3.3(1) \times 10^{-2}$.

Susceptibility Measurements on $TlMnI_3$

χ vs T measurements (see Fig. 8) on a quasi single crystal of $TlMnI_3$ were carried out in the temperature region 1.9–100 K along the three orthorhombic axes. They display a maximum at 6.0 K. Below 6.0 K the various curves of χ vs T diverge sharply, whereas above 6.0 K, χ is isotropic whinin the experimental error. The Néel temperature was taken to be 6.0(2) K, at which temperature $d\chi/dT$ is maximal. From the linear part of $1/\chi$ vs T the Curie–Weiss constant, Θ, was determined to be 10.6(2) K and the effective moment, $\mu_{eff} = 5.99(7)\mu_B$, in good agreement with the theoretical value of 5.92 μ_B.

Two models were used to determine the exchange interaction from the high-temperature data using series expansion according to Dalton and Wood (*11*) for an isotropic Heisenberg system[1]: Model A[2], taking into account the superexchange interactions J_1, J_2, J_3, and J_4 (see Discussion) and assuming that $J_1 + J_2 = J_3 = J_4$, yielded the best fit

[1] In the series expansion, according to Dalton and Wood (*11*), the anisotropy of the system is accounted for by a parameter defined by $\mathcal{H}_N = -\sum_{i,j} J\{S_{i_x}S_{i_x} + \eta\,(S_i^+S_j^- + S_i^-S_j^+)\} - \mu H \sum_{i=1}^{N} S_{i_z}$. For $TlMnI_3$ and $TlFeI_3$, η was taken to be 0.5 and 0.0, yielding an isotropic Heisenberg model and an Ising model, respectively.

[2] The constants for this model in the series expansion according to Dalton and Wood (*11*) are $Q = 10$, $P3 = 3$, $P4 = 7$, $P5 = 12$, $P6 = 67$, $P5a = 6$, $P6a = 0$, $P6b = 21$, $P6c = 17$, and $P6d = 0$.

with $g = 2$ for $J/k = -0.163(1)$ K and model B[3], taking into account $J_{1,2}$ and $J_{1,3}$ (see Discussion) and assuming $J_{1,2} = J_{1,3}$, yielded the best fit for $J/k = -0.40$ K. Both models give a good fit to the experimental data down to 20 K. Below this temperature, Model A gives a better fit as can be seen in Fig. 8. Since the models cannot be discriminated satisfactorily using the susceptibility data, it is more relevant to take the sum of the exchange interactions, zJ/k. This value is determined to be -1.6 K. With $\Theta = 2zS(S+1)J/3k$ (MF theory) zJ/k is calculated to be -1.8 K.

From the magnetization vs field measurements it is evident that, whereas the spins lie in the (0 0 1) plane, the a axis is the most favorable direction. However, at low temperatures $\chi(\|a)$ is larger than $\chi(\|b)$. Also $\chi(\|c)$ shows a temperature dependence which is unexpected since all magnetic moments are perpendicular to the c axis. These effects must be due to the existence of several single crystals in the sample, each with its own orientation, since neutron diffraction results show the magnetic moments to lie in the a–b plane.

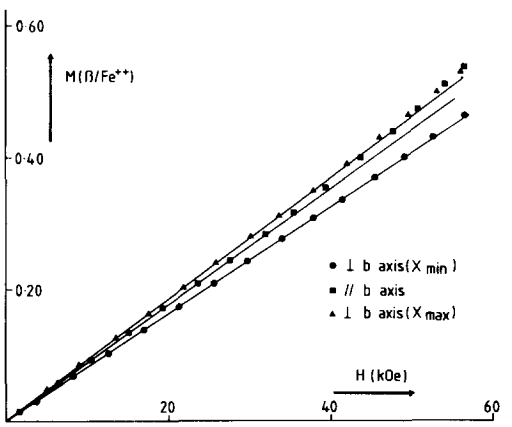

FIG. 9. The magnetization vs the magnetic field curves of a collection of single crystals of $TlFeI_3$ at 4.2 K.

[3] The constants for this model in the series expansion according to Dalton and Wood (*11*) are $Q = 4, P3 = 1, P4 = 1, P5 = 1, P6 = 1, P5a = 1, P6a = 1, P6b = 1, P6c = 1$, and $P6d = 0$.

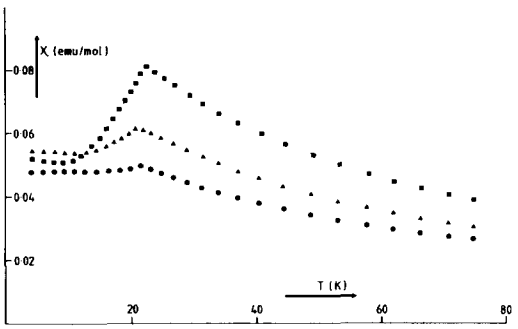

FIG. 10. Susceptibility vs temperature plots measured at a field of 3.9 kOe on a bulk of crystals of $TlFeI_3$ with only an almost common b axis.

Magnetization Measurements on $TlFeI_3$

M vs H measurements (see Fig. 9) were performed at 4.2 K on an aggregate of single crystals of $TlFeI_3$ in three orthogonal directions. From neutron powder diffraction results a magnetization close to zero is expected for low fields parallel to the b axis for a pure single crystal. Probable causes of the deviation from the expected behavior are the contamination of the sample and misorientations.

Susceptibility Measurements on $TlFeI_3$

On the same aggregate of single crystals of $TlFeI_3$, χ vs T measurements were done. The χ vs T curves are depicted in Fig. 10.

Because of impurities and misorientations one can regard these χ vs T measurements as qualitive at best. Evidently the largest drop in χ below T_c is found with a magnetic field along the b axis, in accordance with the neutron diffraction refinements. The drop below T_c in the other two directions is caused probably by misorientations.

Additional χ vs T measurements (see Fig. 11) were performed on a powder of pure $TlFeI_3$. From these data, Θ is found to be

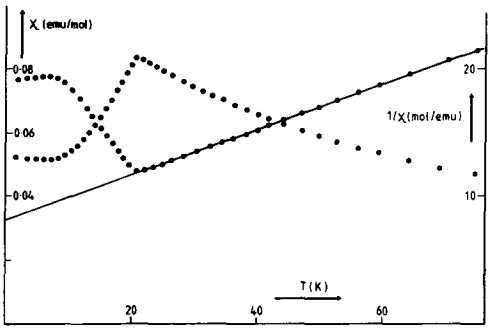

FIG. 11. χ vs T and $1/\chi$ vs T curves of a powder of $TlFeI_3$ measured in a magnetic field of 0.62 kOe.

$-44(3)$ K, yielding $zJ/k = -11(1)$ K with $\Theta = 2zS(S+1)J/3k$. The effective moment was determined as 6.68(5) μ_B. Series expansion fits with an Ising model[1] on the powder data gave the best results using $s = 2$ for model A with $g = 2.69$ and $J/k = -1.0$

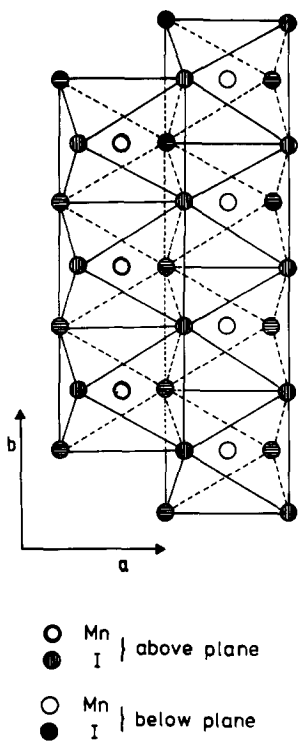

FIG. 12. Double chains of edge-sharing octahedra in $TlMnI_3$ and $TlFeI_3$.

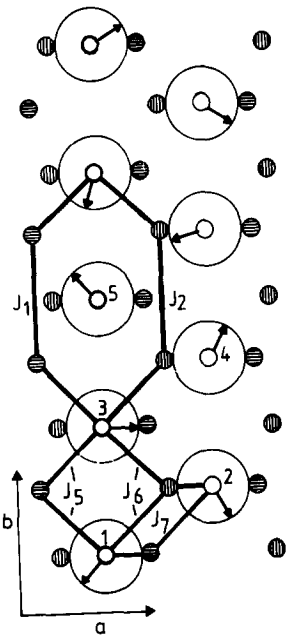

FIG. 13. Exchange interactions in the double chain. J_5, J_6, and J_7 are exchange interactions via one I^- ion and J_1 and J_2 exchange interactions via two I^- ions.

K and for model B with $g = 2.66$ and $J/k = -2.26$ K. This results in $zJ/k = -10(1)$ K and $g = 2.68$. The transition temperature is found to be 21.5(3) K for both the crystal and powder measurements.

Discussion

$TlMnI_3$ and $TlFeI_3$ consist of double chains of edge-sharing MnI_6 (resp. FeI_6) octahedra (see Fig. 12) with Tl^+ ions between the double chains in a nine coordination, a three-capped trigonal prism. Considering the double chain as one chain (Mn(1)–Mn(2)–Mn(3)–Mn(4) . . . (see Fig. 13)) with nearest- and next-nearest-neighbor interac-

tions within this chain, the compound is quasi one dimensional.

The exchange paths between Mn(1) and Mn(2) and between Mn(1) and Mn(3) are almost identical (see Fig. 13 and Table V). Also, the direct exchange between Mn(1) and Mn(2) (distance = 4.28 Å) and between Mn(1) and Mn(3) (distance = 4.27 Å) is expected to be of equal magnitude since their geometry is similar. Therefore the sums of the exchange interactions between the ions Mn(1) and Mn(2), $J_{1,2}$, and between the ions Mn(1) and Mn(3), $J_{1,3}$, are expected to be of equal magnitude. If $J_{1,2}$ and $J_{1,3}$ are ferromagnetic, a collinear structure would occur. If $J_{1,2}$ and $J_{1,3}$ are antiferromagnetic, one would expect the magnetic moments μ(Mn(2)) and μ(Mn(3)) to be as antiparallel as possible to μ(Mn(1)) and to each other. This would lead to a spiral structure in which the directions of μ(Mn(2)), μ(Mn(4)), etc., are completely opposite to those found by neutron diffraction.

Ritter *et al.* (*12*) have demonstrated the dependence of the exchange between two magnetic ions (B) on the angle B–anion–B. This angular dependence (see Fig. 14) suggests that the exchange interaction between two Mn^{2+} ions with an intermediate I^- ion forming a Mn–I–Mn angle of about 90° will be small. Therefore the Mn–I–I–Mn interactions may be important.

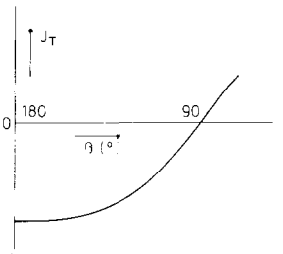

FIG. 14. An example of the dependence of the exchange interaction on the exchange path angle according to Ritter *et al.* (*12*) The sum of the ferromagnetic and antiferromagnetic exchange interactions, J_T vs the exchange path angle, β.

A relatively large Mn–I–I–Mn interaction is expected for a 180°–180° exchange path with small distances. The larger the

TABLE V

THE SUPEREXCHANGE PATHS IN $TnMnI_3$ BETWEEN TWO Mn^{2+} IONS VIA TWO ANIONS OR VIA ONE ANION[a]

A	B	C	D	E	F	G	H
J_1	Mn{0.25}—	2.92—	I(2){0.75}	—4.27—	I(2){1.75}	—2.92—	Mn{2.25}
			137.1		137.1		
J_2	Mn{0.25}—	2.93—	I(3){0.75}	—4.27—	I(3){1.75}	—2.93—	Mn{2.25}
			136.5		136.5		
J_3	Mn{0.25}—	2.93—	I(3){0.75}	—4.09—	I(1){1.25}	—2.81—	Mn{1.25}
			149.4		148.0		
J_4	Mn{0.25}—	2.92—	I(2){0.75}	—3.97—	I(2){1.25}	—2.92—	Mn{1.75}
			148.6		148.6		
J_5	Mn{0.25}—	2.92—	I(2){0.75}	—2.92—	Mn{1.25}		
			94.1				
J_6	Mn{0.25}—	2.94—	I(3){0.75}	—2.94—	Mn{1.25}		
			93.8				
J_7	Mn{0.25}—	2.93—	I(3){0.25}	—2.94—	Mn{0.75}		
			93.8				

[a] The two Mn^{2+} ions with their y positions are given in B and H (B and F for the Mn–I–Mn path) and the two (one) intermediate I^- ions with their y position and the Mn–I–I (Mn–I–Mn) angle in D and F (D). The distances between the ions are given in B, E, and G (B and E).

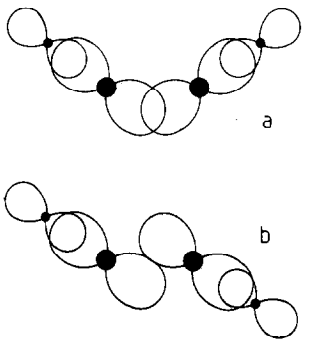

FIG. 15. An example of two superexchange paths between two B^{2+} ions (small circles) via two I^- ions (large circles). Although the distances between the ions and the B–I–I angles are equal the overlap is considerably larger in (a) than in (b).

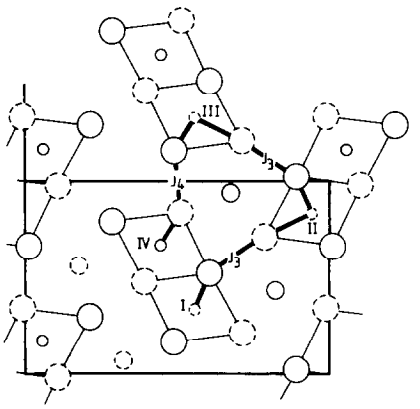

FIG. 16. The exchange interactions between the double chains with exchange path angles larger than 105°. The Roman numerals refer to the chains depicted in Fig. 17.

deviation from 180°, the smaller the overlap of the p orbitals of the I^- ions participating in the exchange mechanism. The exchange paths depicted in Figs. 15a and b can be characterized as a 180°–180° and a 180°–90° exchange path, respectively. Considering only the Mn–I–I–Mn exchange paths (see Table V) with both angles larger than 105°, which are all of the 180°–180° type, it can be seen that there are no important exchange interactions between the Mn^{2+} ions of one chain with the Mn^{2+} ions of the other chain within the same double chain. The direction of the spins in a chain with respect to the spins of the other chain in the double chain will therefore be determined by inter-double-chain interactions (see Figs. 16 and 17). Taking the exchange interactions J_1, J_2, J_3, and J_4 antiferromagnetic, according to the

TABLE VI

THE SUPEREXCHANGE PATHS IN $TlFeI_3$ BETWEEN TWO Fe^{2+} IONS VIA TWO ANIONS WITH ANGLES LARGER THAN 105° AND PATHS VIA ONE ANION[a]

A	B	C	D	E	F	G	H
J_1	Mn{0.25}—	2.82—	I(2){0.75}—	4.21—	I(2){1.75}—	2.82—	Mn{2.25}
			138.3		138.3		
J_2	Mn{0.25}—	2.89—	I(3){0.75}—	4.21—	I(3){1.75}—	2.89—	Mn{2.25}
			136.8		136.8		
J_3	Mn{0.25}—	2.93—	I(3){0.75}—	4.12—	I(1){1.25}—	2.77—	Mn{1.25}
			151.0		147.5		
J_4	Mn{0.25}—	2.82—	I(2){0.75}—	4.01—	I(2){1.25}—	2.82—	Mn{1.75}
			150.3		150.3		
J_5	Mn{0.25}—	2.82—	I(2){0.75}—	2.82—	Mn{1.25}		
			96.6				
J_6	Mn{0.25}—	2.89—	I(3){0.75}—	2.89—	Mn{1.25}		
			93.7				
J_7	Mn{0.25}—	2.85—	I(3){0.25}—	2.89—	Mn{0.75}		
			94.0				

[a] The representation of A, B, C, D, E, F, G, and H is given in Table V.

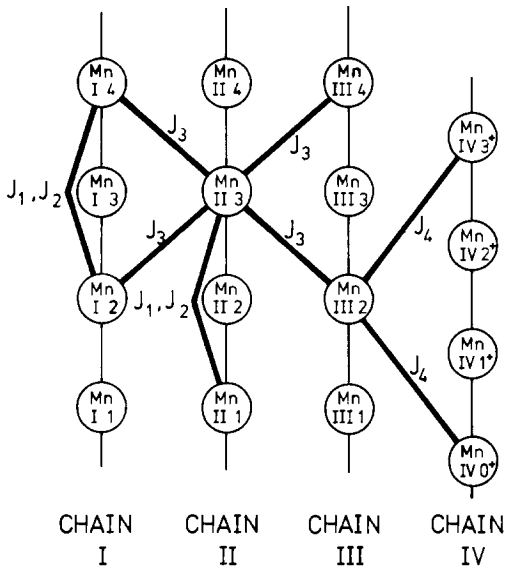

FIG. 17. The chains with the inter-double-chain interactions which determine the spin orientations in the double chain formed by the chains I and IV. The Roman numerals refer to Fig. 16.

predictions of Goodenough (*13*) and Ritter *et al.* (*12*), the spiral structure found for $TlMnI_3$ can be derived. Considering first the interactions between chain I and chain II, as shown in Fig. 18 and starting with a chosen spin direction for Mn(II,3) the spins of Mn(I,2) and Mn(I,4) will be as antiparallel as possible to the spin of Mn(II,3) due to J_3. Because of the exchange interactions J_1 and J_2 between Mn(I,2) and Mn(I,4) the spins of these ions will not be completely antiparallel to the spin of Mn(II,3). The spin directions of half the Mn^{2+} ions of the chains I and II are now fixed with respect to the direction of the spin of Mn(II,3) (see Fig. 18). To determine the spin directions of the other Mn ions in the chains I and II the exchange interaction J_4 between the Mn^{2+} ions in the chains 0 and I is used (Fig. 19). Considering the exchange interaction between $Mn(0,2^+)$ and Mn(I,1) and Mn(I,4), respectively, the spins of Mn(I,1) and Mn(I,4) will be as antiparallel as possible to the spin of $Mn(0,2^+)$ and furthermore as there is no Mn–I–I–Mn interaction between Mn(I,1) and Mn(I,4) the spins of these two ions will be as parallel as possible. Consequently the spin of Mn(I,n) will be as parallel as possible to the spins of Mn(I,n + 3) and Mn(I,n − 3). Therefore the spin of Mn(I,n) will be completely parallel to the spin of Mn(II,n) (Fig. 19). A similar derivation can be given for the direction of the spin of Mn(III,3), which must be parallel to the spin of Mn(II,3) as well as for the direction of the spin of a virtual Mn^{2+} ion half between $Mn(IV,2^+)$ and $Mn(IV,3^+)$, which must be parallel to the spin of Mn(III,3). All this results in a spiral structure with ferromagnetic (0 1 0) planes.

The relative magnitudes of J_1, J_2, J_3, and J_4 will determine the length of the propagation vector **k**. The pitch of the spiral shows J_1 and J_2 to be small compared to J_3 and J_4. This difference in magnitude is probably caused by the larger I–I distances and the smaller angles in the exchange paths of J_1 and J_2.

With the same antiferromagnetic ex-

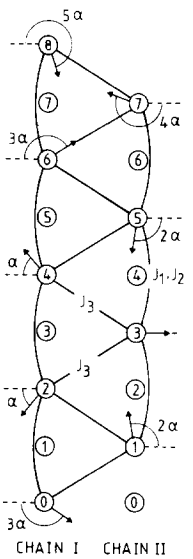

FIG. 18. The spin orientations in the chains I and II, when the exchange interactions J_1, J_2, and J_3 are taken into account.

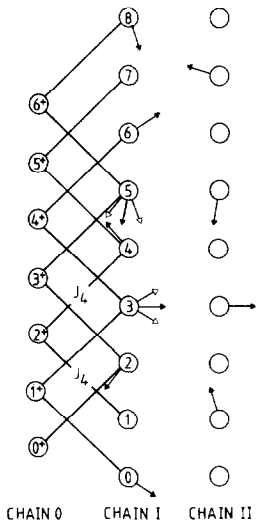

FIG. 19. The spin orientation in chain I when the exchange interactions J_1, J_2, J_3, and J_4 are taken into account.

change interactions J_1, J_2, J_3, and J_4 the magnetic structure of $TlFeI_3$ can be derived when an anisotropy stronger than the exchange interactions is assumed. Assuming that $J_3 > J_1 + J_2$ the spins of the Fe^{2+} ions in chain II (see Fig. 20) are completely parallel to each other and completely antiparallel to the spins of the ions in chain I. Since the interactions between the Fe^{2+} ions in the chain III and the chains II and IV are antiferromagnetic, the spins of the Fe^{2+} ions in the chains II and IV will be antiparallel to those in the chains I and III. All this results in a magnetic structure as found for $TlFeI_3$.

Two magnetic structures of isomorphous Cl compounds have been reported, viz., $KMnCl_3$ (*14*) and $KFeCl_3$ (*15*). $KMnCl_3$ has a structure similar to that of $TlMnI_3$ however with the spins in the a–c plane. Consequently this structure can be derived with the exchange interactions J_1, J_2, J_3, and J_4. It is not possible to derive the magnetic structure of $KFeCl_3$ (*15*) with the same assumptions as those for $TlFeI_3$. $KFeCl_3$ consists of puckered ferromagnetic (0 0 1) planes coupled antiferromagnetically whereby the magnetic moments are directed along the b axis. The Cl^- ions have a less covalent character resulting in smaller exchange interactions via two anions. Also the distance between the B^{2+} ions in the chlorine compounds is smaller. If the exchange interactions between nearest-neighbor B^{2+} ions are stronger than the exchange interactions via two anions the orientations of the spins in a double chain will be determined by nearest-neighbor interactions, viz., intra-double-chain interactions. This is probably the case in $KFeCl_3$. This would also explain the one-dimensional behavior above T_c of $KFeCl_3$, whereas $KMnCl_3$ does not exhibit such behavior.

The sharp maxima in the χ vs T curves of $TlMnI_3$ and $TlFeI_3$ are in accordance with the assumption that superexchange interactions exist in all directions resulting in a three-dimensional magnetic system. Experimental values (*16*) of T_c/Θ, being a measure for the dimensionality of the compound, for a one dimensional $s = 5/2$ Heisenberg system are found to be smaller than 0.1, whereas 0.38–0.48 and 0.70–0.79 are the values T_c/Θ found for two- and three-dimensional $s = 5/2$ systems, respectively. For $TlMnI_3$ and $TlFeI_3$, T_c/Θ are found to be 0.55 and 0.49. These values have to be corrected for the existance of

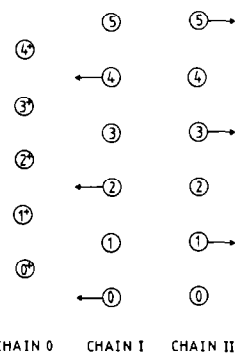

FIG. 20. The spin orientation in the chains I and II when the exchange interactions J_1, J_2, and J_3 are taken into account and a strong anisotropy is assumed.

competing exchange interactions since T_c is proportional to $\sum_{a,i>j} J_a \mathbf{S}_i \cdot \mathbf{S}_j$ and Θ is proportional to $\sum_{a,i>j} J_a S_i S_j$. Correction for these competing exchange interactions would lead to T_c/Θ values close to the experimental values of three-dimensional Heisenberg and Ising systems.

The transition to a three-dimensional magnetic ordering takes place at a relatively much higher temperature for $TlMnI_3$ (T = 6.0 K) than for $KMnCl_3$ (T = 2.1K). This effect must be due to the more covalent character of the I^- ions leading to stronger superexchange interactions. This effect is in accordance with the assumption that superexchange interactions via two I^- ions are the most important.

A similar increase in T_c occurs in quasi-one-dimensional compounds with the $BaNiO_3$ structure. Comparing, for instance, $CsMnBr_3$ (*17*) with $J/k = -9.6$ K and T = 8.3 K and $CsMnI_3$ (*18*) with $J/k = -9.1$ K and T = 11.1 K, one finds that the introduction of I^- ions causes a weaker intrachain exchange J/k and a stronger interchain exchange (proportional to T_c). The most important intrachain exchange interaction, the direct exchange interaction, will be smaller in $CsMnI_3$ due to a smaller overlap of the t_{2g} orbitals of nearest-neighbor Mn^{2+} ions. Although the distance between the chains is larger in $CsMnI_3$ a stronger interchain exchange interaction occurs due to the larger covalency of the I^- ions.

The conclusion is that the title compounds are three-dimensional antiferromagnetic systems, first because the magnetic structures can be well understood if three-dimensional interactions are considered to be dominating, and second because of the T_c/Θ values and the χ vs T curves. Furthermore, the strong increase in T_c on introduction of more covalent anions is in accordance with this conclusion.

Acknowledgments

The author wishes to thank Dr. D. J. W. IJdo, Dr. L. J. de Jongh, and Dr. R. A. G. de Graaff for helpful discussions and a critical reading of the manuscript, and Mr. J. Strang of the Energieonderzoek Centrum Nederland for performing the neutron diffraction experiments.

References

1. H. J. SEIFERT AND K. H. KISCHKA, *Thermochim. Acta* **27**, 85 (1978).
2. H. W. ZANDBERGEN, G. C. VERSCHOOR, AND D. W. J. IJDO, *Acta. Crystallogr. Sect. B* **35**, 1425 (1979).
3. H. W. ZANDBERGEN, *Acta Crystallogr. Sect. B* **35**, 2852 (1979).
4. H. P. HAUPT, F. HUBER, AND H. PREUT, *Z. Anorg. Allg. Chem.* **408**, 209 (1974).
5. C. K. MOLLER, *Mat. Fys. Med. K. Dan. Vidensk. Selsk.* **32**, 1 (1959).
6. Compilation, Bacon, 1977.
7. R. E. WATSON AND A. J. FREEMAN, *Acta Crystallogr.* **14**, 27 (1961).
8. H. M. RIETVELD, *J. Appl. Crystallogr.* **2**, 65 (1969).
9. H. T. WITTEVEEN, Thesis, University of Leiden, 1973.
10. J. KANAMORI, *in* "Magnetism" (G. T. Rado and H. Suhl, Eds.), Vol. 1, Academic Press, New York (1963).
11. D. W. DALTON AND N. W. WOOD, *J. Phys. C* **5**, 1675 (1972).
12. R. RITTER, L. JANSEN, AND E. LOMBARDI, *Phys. Rev. B* **8**, 2139 (1973)
13. J. B. GOODENOUGH, "Magnetism and the Chemical Bond" (F. A. Cotton, Ed.), Interscience, New York (1963).
14. E. GUREWITZ, A. HOZAWITZ, AND H. SHAKED, *Phys. Rev. B* **20**, 4544 (1979).
15. E. GUREWITZ AND H. SHAKED, *Acta Crystallogr., Sect. A* **28**, 280 (1972).
16. L. J. DE JONGH AND A. R. MIEDEMA, *Advan. Phys.* **23**, 1 (1974).
17. M. EIBSCHUETZ, R. C. SHERWOOD, F. S. L. HSU, AND D. E. COX, *in* "Proceedings, AIP Conference on Magnetism and Magnetic Materials," 684 (1972).
18. H. W. ZANDBERGEN, *J. Solid State Chem.* **35**, 367 (1980).
19. "International Tables for X-Ray Crystallography," Vol II, p. 241, Kinoch Press, Birmingham.